Effect of Surface Impurities on Tracer Diffusion in Insulators*

Michael D. Feit,† Joan L. Mitchell, and David Lazarus
Department of Physics and Materials Research Laboratory, University of Illinois, Urbana, Illinois 61801
(Received 20 February 1973)

In self-diffusion experiments performed on insulators in which a radioactive tracer is deposited as a thin source, heterovalent impurities, initially present on the sample surface or in the tracer solution, may diffuse into the sample along with the tracer. This effect may be important, even for very small amounts of impurity, since each heterovalent ion entering the lattice automatically introduces one or more extrinsic vacancies to maintain charge neutrality. If the extrinsic-vacancy concentration is comparable to the thermal-equilibrium concentration, this effect can cause a marked deviation from the expected Gaussian behavior. A model is developed for iteratively solving the nonlinear diffusion equation for the case of an unknown divalent impurity co-diffusing with a monovalent tracer in an alkali-halide lattice. The solutions show a strong curvature in the tracer profiles, the amount of curvature depending on the amount and relative diffusivity of the impurity, and on the diffusion time. The model permits fairly precise determination of the "true" tracer diffusion coefficient and approximate values for the concentration and diffusivity of the impurity. Experimental results are presented which show good agreement between the predicted time dependence of the model and experiment for "carrier-free" Na^{22} diffusing in NaCl.

I. INTRODUCTION

Although considerable attention has been directed toward understanding the modification of self-diffusion by randomly distributed impurities in otherwise pure materials, little effort has been directed toward consideration of the effect of nonhomogeneous impurity distributions introduced by the environment or by a tracer solution.

Such effects are particularly important in understanding the results of tracer-diffusion experiments in ionic crystals, since heterovalent impurities which may co-diffuse with the tracer strongly influence the vacancy concentration. For definiteness, we consider the simultaneous diffusion of solvent tracer atoms and divalent impurities for the alkali halides. Although the number of impurity atoms which enter the crystal may be quite small, local concentrations may be comparable to the thermal vacancy concentration. In this case, a large effect is expected since each divalent impurity automatically brings in an extrinsic vacancy to maintain charge neutrality. Curved penetration plots attributed to such effects have been observed in alkali-halide self-diffusion experiments,[1] and the plots appear to become more curved at high pressure.[2] Similar effects have also been reported for the diffusion of divalent cations in monovalent ionic lattices,[3,4] and, more recently, numerical calculations[5] based on the Lidiard model[6] have reproduced the curved penetration plots seen experimentally. These numerical calculations show that the curvature grows worse as the amount of divalent ion deposited is increased, or as the diffusion anneal time is decreased.

The present paper is devoted to a theoretical treatment of self-diffusion in an ionic crystal assuming that a divalent impurity diffuses into the sample along with the tracer. We derive an analytic approximate expression for the penetration profile which can be compared to experiment, the relevant parameters being the amount of impurity and the tracer and impurity diffusivities. We assume that the local tracer diffusivity depends linearly on the local impurity concentration, a reasonable approximation for divalent impurities in the alkali halides.

The main part of the paper, Sec. II, is concerned with finding an asymptotic (in time) solution to the appropriate diffusion equation (valid to all orders in the penetration distance). First, an exact solution to first order in the impurity concentration is found for the tracer penetration profile when the impurity distribution is Gaussian. The tracer profile is curved, the curvature increasing with the amount of impurity or decreasing diffusion time. In particular, it is found that one may measure a penetration profile that is nearly Gaussian over several orders of magnitude, but whose limiting slope gives an appreciable error for the tracer diffusivity. Next, the effect of the extra vacancies on the impurity's distribution is considered, and an iterative procedure is used to find a converging solution for the impurity distribution. This non-Gaussian impurity distribution makes slight modifications in the solution of the diffusion equation for the tracer concentration. Finally, an approximate solution to second order is derived.

Section III uses the results of Sec. II to interpret three penetration plots, all taken at the same temperature, but for different anneal times. The implication of these results for the interpretation of

tracer diffusion experiments is discussed in Sec. IV.

II. SOLUTION OF THE DIFFUSION EQUATION

In what follows, we shall assume that the local tracer diffusivity is proportional to the local vacancy concentration, and, therefore, is a linear function of the local impurity concentration. We shall use the following scheme to avoid the complexities of having to consider coupled flux equations: In the first step, the impurity is assumed to have a Gaussian distribution. The resulting equation for the asymptotic Fourier transform of the tracer profile can be solved exactly to first order.

In the second step, the impurity distribution is no longer assumed to be Gaussian, since it is similarly affected by the extra vacancies. For this case the excess vacancy concentration is proportional to the local concentration of the divalent ion, so the first-order solution is iterated until it converges. This non-Gaussian distribution of the extra vacancies is used to find the tracer-penetration profile which is still exact to first order and approximate to second order in the impurity concentration. Then second-order terms are included in the final iterated solution for the impurity, and an improved tracer-penetration profile is found.

For very long anneals, only the first-order Gaussian impurity solution should be necessary; for shorter anneals, the full expression is needed, while for a very large effect the present perturbative treatment breaks down.

A. Formal Development for Any Impurity Distribution

We wish to find the solution for the tracer concentration $c_t(x,t)$ on the infinite strip $-\infty < x < \infty$ for the diffusion equation

$$\frac{\partial c_t}{\partial t} = \frac{\partial}{\partial x}\left(D_t \frac{\partial c_t}{\partial x}\right), \tag{1}$$

with the usual δ-function initial condition. We take the true tracer-diffusion coefficient to be

$$D_t = D_{t0} + \Delta(x,t), \tag{2}$$

where D_{t0} is the constant diffusivity determined by the homogeneous, intrinsic vacancies and $\Delta(x,t)$ is the position and time-dependent part of the diffusivity which is proportional to the impurity's distribution. The desired solution may be expanded in terms of the eigenfunctions of the corresponding separable $D_t = D_{t0}$ problem. This results in a set of linear equations for the expansion coefficients in terms of matrix elements of the perturbation in the usual way. To this end, we define the differential operators

$$d = d_0 + \delta, \tag{3a}$$

with

$$d_0 = D_{t0}\frac{\partial^2}{\partial x^2} \tag{3b}$$

and

$$\delta = \left(\frac{\partial \Delta}{\partial x}\right)\frac{\partial}{\partial x} + \Delta\frac{\partial^2}{\partial x^2}, \tag{3c}$$

so that Eq. (1) may be written

$$\frac{\partial c_t}{\partial t} = d c_t. \tag{4}$$

Since the eigenfunctions of the D_{t0} problem are of the type[7]

$$\phi_k = \exp[ikx/(D_{t0})^{1/2} - k^2 t], \tag{5}$$

we look for a solution of the type

$$c_t(x,t) = \int_{-\infty}^{\infty} dk\, A_k(t) \exp[ikx/(D_{t0})^{1/2} - k^2 t]. \tag{6}$$

The equation for the A_k's is found by substituting Eq. (6) into Eq. (4), multiplying the resulting expression by $\exp[-iqx(D_{t0})^{1/2}]$, and integrating over x. This yields

$$\dot{A}_q(t) e^{-q^2 t} = \int_{-\infty}^{\infty} dk\, A_k(t) e^{-k^2 t} \langle q \mid \delta \mid k \rangle, \tag{7a}$$

where $\dot{A}$ denotes the time derivative of A, and

$$\langle q \mid \delta \mid k \rangle \equiv \frac{1}{2\pi}\int_{-\infty}^{\infty} \frac{dx}{(D_{t0})^{1/2}} \exp\left(-\frac{iqx}{(D_{t0})^{1/2}}\right) \times \delta \exp\left(\frac{ikx}{(D_{t0})^{1/2}}\right). \tag{7b}$$

Note that this is a general expression for any $\Delta(x,t)$. To go further, we have to assume a functional form for $\Delta(x,t)$ (i.e., an impurity distribution). We assume that

$$\Delta(x,t) = \gamma c_{\text{imp}}, \tag{8}$$

where γ is a proportionality constant which relates the impurity distribution to $\Delta(x,t)$.

B. Gaussian Impurity Distribution

If the impurity diffusivity D_{i0} is first considered to be unaffected by the extra vacancies, then the impurity's concentration c_{imp} would have the Gaussian dependence expected for diffusion from a thin source into a homogeneous material:

$$c_{\text{imp}} = \frac{M \exp(-x^2/4D_{i0}t)}{A(\pi 4 D_{i0} t)^{1/2}}, \tag{9}$$

where M is the total number of impurity atoms and A is the area. In this case,

$$\delta \exp\left(\frac{ikx}{(D_{t0})^{1/2}}\right) = \left(\frac{-x}{2D_{i0}t}\ \frac{ik}{(D_{t0})^{1/2}} - \frac{k^2}{D_{t0}}\right) \times \frac{\gamma M \exp(-x^2/4D_{i0}t)\exp[ikx/(D_{t0})^{1/2}]}{A(\pi 4 D_{i0} t)^{1/2}} \tag{10a}$$

and

$$\langle q \mid \delta \mid k \rangle = -kqC\pi^{-1/2} e^{-(k-q)^2 rt}. \tag{10b}$$

Here

$$C=\gamma M/AD_{t0}(\pi 4D_{t0})^{1/2} \tag{11a}$$

and

$$r=D_{i0}/D_{t0} \tag{11b}$$

are constants. Equation (7a) now becomes

$$\dot{A}_q(t)=-qC\pi^{-1/2}\int_{-\infty}^{\infty} dk\, k A_k(t) \times \exp[(q^2-k^2)t-(k-q)^2 rt]. \tag{12}$$

We cannot use the usual method of time-dependent perturbation theory to treat Eq. (12) since the initial distribution is not one of the eigenfunctions (plane waves), but, rather, a linear combination of all of them. Noting that A_k must be an even function of k [Eq. (6)] with the initial condition $A_k(0)=1$,[7] we set

$$A_k(t)=\exp\left(-\sum_{n=1}^{\infty} a_n(t)k^{2n}\right), \tag{13}$$

and solve for the a_n.

Since C multiplies the integral in Eq. (12), the first-order equation for a_n is simply

$$\sum_{n=1}^{\infty}\dot{a}_n q^{2n}=qC\pi^{-1/2}\int_{-\infty}^{\infty} dk\, k\exp[(q^2-k^2)t-(k-q)^2 rt] =q^2 Cr(r+1)^{-3/2}t^{-1/2}e^{q^2t/(r+1)}, \tag{14}$$

so that, after expanding the right-hand side of Eq. (14) in powers of q^2, we have

$$\dot{a}_n=Cr(r+1)^{-n-1/2}t^{n-3/2}/(n-1)! \tag{15a}$$

and

$$a_n=Cr[t(r+1)]^{-1/2}\left(\frac{t}{r+1}\right)^n \frac{1}{(n-1)!(n-\frac{1}{2})}. \tag{15b}$$

We can find a simple expression for the tracer concentration $c_t(x,t)$ through the use of the formal result

$$e^{-k^{2n}a_n-k^2t}=\left(\sum_m \frac{(-k^{2n}a_n)^m}{m!}\right)e^{-k^2t} =\left(\sum_m (-1)^{m(n+1)}\frac{a_n^m}{m!}\frac{\partial^{nm}}{\partial t^{nm}}\right)e^{-k^2t} \tag{16a}$$

$$=\exp\left((-1)^{n+1}a_n\frac{\partial^n}{\partial t^n}\right)e^{-k^2t}, \tag{16b}$$

where the exponential operator of Eq. (16b) is defined as the operator of Eq. (16a). Then, from Eqs. (6) and (13), we see that c_t can be written

$$c_t(x,t)=\int_{-\infty}^{\infty} dk\exp\left(-k^2t-\sum k^{2n}a_n+\frac{ikx}{(D_{t0})^{1/2}}\right) =\exp\left(-\sum_{n=1}(-1)^n a_n\frac{\partial^n}{\partial t^n}\right)\left(\frac{\pi}{t}\right)^{1/2}\exp\left(-\frac{x^2}{4D_{t0}}\right), \tag{17}$$

with the first-order form

$$c_t(x,t)\approx\left(1-\sum_n(-1)^n a_n\frac{\partial^n}{\partial t^n}\right)\left(\frac{\pi}{t}\right)^{1/2}\exp\left(-\frac{x^2}{4D_{t0}t}\right). \tag{18}$$

The necessary derivatives are easily evaluated. If we call

$$\phi=(\pi/t)^{1/2}e^{-z_0^2} \tag{19a}$$

and

$$z_0^2=x^2/4D_{t0}t, \tag{19b}$$

then

$$\phi^{-1}\frac{\partial^n\phi}{\partial t^n}=(-2t)^{-n}(2n-1)!!\left(1-2nz_0^2+\tfrac{2}{3}n(n-1)z_0^4 +\cdots+(-1)^k\frac{n(n-1)\cdots(n-k+1)(2z_0^2)^k}{k!(2k-1)!!} +\cdots+(-1)^n\frac{(2z_0^2)^n}{(2n-1)!!}\right). \tag{20}$$

From Eq. (15b) we see that

$$\frac{a_n}{(2t)^n}=Cr[t(r+1)]^{-1/2}[2(r+1)]^{-n}\frac{2}{(n-1)!(2n-1)}, \tag{21}$$

so Eq. (18) becomes

$$c_t(x,t)\approx\left[1-2Cr[t(r+1)]^{-1/2} \times\left(S_0(\beta)+\sum_{k=1}^{\infty}S_k(\beta)\frac{(-2z_0^2)^k}{k!(2k-1)!!}\right)\right]\phi(x,t); \tag{22}$$

in the above,

$$\beta=[2(r+1)]^{-1}, \tag{23a}$$

$$S_0(\beta)=\sum_{n=1}^{\infty}\frac{\beta^n(2n-1)!!}{(2n-1)(n-1)!}, \tag{23b}$$

and

$$S_k(\beta)=\sum_{n=1}^{\infty}\frac{\beta^n(2n-1)!!}{(2n-1)(n-1)!}n(n-1)\cdots(n-k+1), \qquad k>0. \tag{23c}$$

The sums $S_k(\beta)$ may be evaluated by noting that

$$S_0=\frac{\beta}{(1-2\beta)^{1/2}}=\left(\frac{r}{r+1}\right)^{1/2}\frac{1}{2r} \tag{24a}$$

and

$$S_k(\beta)=\beta^k\frac{\partial^k S_0(\beta)}{\partial\beta^k}=(1-2\beta)^{1/2}\left(\frac{\beta}{1-2\beta}\right)^k \times(2k-1)!!\left(\frac{k}{2k-1}+\frac{\beta}{1-2\beta}\right) =\left(\frac{r}{r+1}\right)^{1/2}\left(\frac{1}{2r}\right)^k(2k-1)!!\left(\frac{k}{2k-1}+\frac{1}{2r}\right). \tag{24b}$$

The general form for S_k may be verified by mathematical induction;

$$\left(S_0(\beta)+\sum_{k=1}^{\infty} S_k(\beta)\,\frac{(-2z_0^2)^k}{k!(2k-1)!!}\right)=\left(\frac{r}{r+1}\right)^{1/2}\left(\sum_{k=1}^{\infty}\frac{(-z_0^2/r)^k}{(k-1)!\,(2k-1)}+\frac{1}{2r}\sum_{k=0}^{\infty}\frac{(-z_0^2/r)^k}{k!}\right)$$

$$=\frac{1}{2}\left(\frac{r}{r+1}\right)^{1/2}\left\{-\left(\frac{\pi z_0^2}{r}\right)^{1/2}\operatorname{erf}\left[\left(\frac{z_0^2}{r}\right)^{1/2}\right]+\frac{e^{-z_0^2/r}}{r}\right\}. \tag{25}$$

Finally, using the above in Eq. (22), we see that the asymptotic form of $\ln c_t$ is given by

$$\ln c_t(x,t)=\ln c_0(t)-z_0^2+\frac{Ct^{-1/2}r^{3/2}}{r+1}$$

$$\times\left\{\left(\frac{\pi z_0^2}{r}\right)^{1/2}\operatorname{erf}\left[\left(\frac{z_0^2}{r}\right)^{1/2}\right]-\frac{e^{-z_0^2/r}}{r}\right\}. \tag{26}$$

This solution for the tracer concentration c_t, exact to first order in the impurity concentration, can be written

$$c_t(x,t)=c_0(t)\exp\left(-\frac{x^2}{4D_{t0}t}+\frac{\alpha 2r^{3/2}z}{r+1}\right.$$

$$\left.\times\int_0^z E_0(\xi)\,d\xi-\frac{\alpha r^{1/2}}{r+1}E_0(z)\right), \tag{27a}$$

where

$$z^2=x^2/4D_{t0}t=z_0^2/r, \tag{27b}$$

$$E_0(z)=e^{-z^2}/\int_{-\infty}^{\infty}e^{-z^2}dz=\pi^{-1/2}e^{-z^2}, \tag{27c}$$

and

$$\alpha(t)=\gamma M/AD_{t0}(4D_{t0}t)^{1/2}=(\pi/t)^{1/2}C. \tag{27d}$$

The integral $\int_{-\infty}^{\infty}e^{-z^2}dz$ enters from the normalization condition that

$$\int_{-\infty}^{\infty}c_{imp}dx=M/A, \tag{28a}$$

where

$$c_{imp}=Me^{-z^2}/A(\pi 4D_{t0}t)^{1/2}=ME_0(z)/A(4D_{t0}t)^{1/2}. \tag{28b}$$

C. Iterative Solution for Non-Gaussian Impurity Distribution

If the diffusion time is short or the concentration is large, then considering the concentration of the impurity, c_{imp}, as a Gaussian distribution is a poor approximation since the impurity's diffusivity should be similarly affected by the extrinsic vacancies. Thus, we take, as a better approximation,

$$D_i=D_{i0}(1+\gamma c_{imp}/D_{i0}), \tag{29a}$$

or in terms of α,

$$D_i=D_{i0}[1+(\alpha/r^{3/2})E_0(z)]. \tag{29b}$$

The solution to the diffusion equation for the impurity is then given by Eq. (27a) where D_{t0} is replaced by D_{i0} and $r=1$. Since $\alpha\propto(D_{t0})^{-3/2}$, α is replaced by $\alpha/r^{3/2}$. The total amount of impurity remains fixed so one must renormalize; then

$$c_{imp}=[M/A(4D_{i0}t)^{1/2}]\,E_1(z,t), \tag{30a}$$

where

$$E_1(z,t)=\exp\left(-z^2+\frac{\alpha z}{r^{3/2}}\int_0^z E_0(\xi)\,d\xi-\frac{\alpha}{2r^{3/2}}E_0(z)\right)\Big/\int_{-\infty}^{\infty}\exp\left(-z^2+\frac{\alpha z}{r^{3/2}}\int_0^z E_0(\xi)\,d\xi-\frac{\alpha}{2r^{3/2}}E_0(z)\right)dz. \tag{30b}$$

The explicit t dependence in $E_1(z,t)$ comes from $\alpha(t)$. A still better approximation for the impurity's diffusivity would be

$$D_i=D_{i0}[1+(\alpha/r^{3/2})E_1(z,t)]. \tag{31}$$

The solution for the impurity concentration to first order is then

$$c_{imp}=[M/A(4D_{i0}t)^{1/2}]E_2(z,t), \tag{32a}$$

where

$$E_2(z,t)=\exp\left(-z^2+\frac{\alpha z}{r^{3/2}}\int_0^z E_1(\xi,t)\,d\xi-\frac{\alpha}{2r^{3/2}}E_1(z,t)\right)\Big/\int_{-\infty}^{\infty}\exp\left(-z^2+\frac{\alpha z}{r^{3/2}}\int_0^z E_1(\xi,t)\,d\xi-\frac{\alpha}{2r^{3/2}}E_1(z,t)\right)dz. \tag{32b}$$

This iteration procedure can be repeated indefinitely; after n iterations

$$c_{imp}=[M/A(4D_{i0}t)^{1/2}]E_n(z,t), \tag{33a}$$

where

$$E_n(z,t)=\exp\left(-z^2+\frac{\alpha z}{r^{3/2}}\int_0^z E_{n-1}(\xi,t)\,d\xi-\frac{\alpha}{2r^{3/2}}E_{n-1}(z,t)\right)\Big/\int_{-\infty}^{\infty}\exp\left(-z^2+\frac{\alpha z}{r^{3/2}}\int_0^z E_{n-1}(\xi,t)\,d\xi-\frac{\alpha}{2r^{3/2}}E_{n-1}(z,t)\right)dz. \tag{33b}$$

The solutions converge after a few iterations; the number of iterations necessary depends upon the magnitude of the factor $\alpha/r^{3/2}$. For $\alpha/r^{3/2}<1$, the solutions converge in three iterations. We can then use this iterated solution for c_{imp} as an improved approximation for the distribution of the extra vacancies; then, for the tracer,

$$D_t = D_{t0}[1+(\alpha/r^{1/2})E_n(z,t)]\,, \tag{34a}$$

which gives

$$c_t(x,t) = c_0(t)\exp\left(-\frac{x^2}{4D_{t0}t}+\frac{\alpha 2r^{3/2}}{r+1}z \times\int_0^z E_n(\xi,t)\,d\xi - \frac{\alpha r^{1/2}E_n(z,t)}{r+1}\right)\,. \tag{34b}$$

This expression for c_t is still exact to first order in α. Note that α is the parameter which shows that the effect increases in direct proportion with the impurity concentration, inversely with the square root of time, and inversely with D_{t0} to the $\frac{3}{2}$ power.

D. Approximate Second-Order Solution

The first-order expression for c_t, Eq. (34b), is adequate for $\alpha/r^{1/2}<0.5$. However, for large α the rapidly varying term $-\alpha r^{1/2}(r+1)^{-1}E_n(z,t)$ dominates in the near-surface region and gives a downward spike. Thus, the first-order solution gives a maximum of the tracer concentration displaced from the origin, for large α, rather than at the surface. The dotted lines in Fig. 3 which show the first-order expression for c_t for the best-fit values of α, r, and D_{t0} illustrate how this downward spike increases with increasing α. It thus becomes apparent that higher-order terms are needed for $\alpha/r^{1/2}\gtrsim 1$.

To find an approximate solution to second order, including terms in α^2, we assume that terms of order α^2 are additive in $\ln c_t$. Then,

$$c_t = c_{t1}e^{\alpha^2 G(x,t)}\,, \tag{35}$$

where $G(x,t)$ is some unknown function and c_{t1} is the first-order solution given by Eq. (34b).

The diffusion equation [Eq. (1)], where D_t is given by Eq. (34a), then gives

$$e^{\alpha^2 G}\frac{\partial c_{t1}}{\partial t}+\alpha^2 c_t\frac{\partial G}{\partial t}+Gc_t\frac{\partial \alpha^2}{\partial t} = D_t\left[e^{\alpha^2 G}\frac{\partial^2 c_{t1}}{\partial x^2}+\alpha^4 c_t\left(\frac{\partial G}{\partial x}\right)^2+\alpha^2 c_t\frac{\partial^2 G}{\partial x^2}+2\alpha^2 e^{\alpha^2 G}\frac{\partial c_{t1}}{\partial x}\frac{\partial G}{\partial x}\right] + \frac{D_{t0}\alpha}{r^{1/2}}\frac{\partial E_n}{\partial x}\left(e^{\alpha^2 G}\frac{\partial c_{t1}}{\partial x}+\alpha^2 c_t\frac{\partial G}{\partial x}\right)\,. \tag{36}$$

After taking derivatives, all terms of zero or first order in α cancel exactly. By collecting terms of order α^2 and cancelling the common factor $\alpha^2 c_t$, we obtain the following approximate differential equation for $G(x,t)$:

$$-\frac{G}{t}+\frac{\partial G}{\partial t} = D_{t0}\frac{\partial^2 G}{\partial x^2}-\frac{x}{t}\frac{\partial G}{\partial x}+\frac{r^2}{(r+1)^2 t}\left(\int_0^z E_n(\xi,t)\,d\xi\right)^2-\frac{zE_n(z,t)}{(r+1)t}\int_0^z E_n(\xi,t)\,d\xi-\frac{z^2E_n^2(z,t)(r+2)}{rt} + \frac{E_n^2(z,t)(2r+1)}{2r(r+1)t}+\frac{zE_n(z,t)\int_0^z E_{n-1}(\xi,t)\,d\xi}{2r^2(r+1)t}+\frac{z^2E_n(z,t)E_{n-1}(z,t)(r+2)}{r^2(r+1)t}+\frac{E_n(z,t)E_{n-1}(z,t)(r-3)}{4r^2(r+1)t}\,. \tag{37}$$

$E_{n-1}(z,t)$ is proportional to the extrinsic-vacancy distribution which affects the impurity diffusivity. Since $E_n(z,t)$ is a better approximation to the extrinsic-vacancy distribution, we can change $E_{n-1}(z,t)$ to $E_n(z,t)$ and then combine terms. As a trial solution let

$$G(x,t) = A\left[\int_0^z E_n(\xi,t)\,d\xi\right]^2+BzE_n(z,t)\int_0^z E_n(\xi,t)\,d\xi + CE_n^2(z,t)+Fz^2E_n^2(z,t)\,. \tag{38}$$

If we keep only zero-order terms in the derivatives of $G(x,t)$ and convert E_{n-1} into E_n, Eq. (37) then gives

$$0=\left(\int_0^z E_n(\xi,t)\,d\xi\right)^2\left(\frac{A}{t}+\frac{r^2}{(r+1)^2 t}\right) \tag{39a}$$

$$+\frac{z^3E_n(z,t)\int_0^z E_n(\xi,t)\,d\xi}{t}\left(B\frac{r+1}{r}\right) \tag{39b}$$

$$+\frac{zE_n(z,t)\int_0^z E_n(\xi,t)\,d\xi}{t}\left[-\frac{A(r+1)}{r}+\frac{B}{2}\left(\frac{r-3}{r}\right) -\frac{1}{r+1}+\frac{1}{2r^2(r+1)}\right] \tag{39c}$$

$$+\frac{E_n^2(z,t)}{t}\left(\frac{A}{2r}+\frac{B}{2r}+\frac{C(r-1)}{r}+\frac{F}{2r}+\frac{2r+1}{2r(r+1)} +\frac{r-3}{4r^2(r+1)}\right) \tag{39d}$$

$$+\frac{z^2E_n^2(z,t)}{t}\left(\frac{-B}{2r}(r+3)+\frac{2C}{r}(r+2)-\frac{5F}{r}\right.$$

$$-\frac{r+2}{r}+\frac{r+2}{r^2(r+1)}\Bigg) \quad (39e)$$

$$+\frac{z^4E_n^2(z,t)}{t}\left(\frac{2F}{r}(r+2)\right). \quad (39f)$$

[Note that since a solution requires that Eqs. (39a)–(39f) be identically zero and since there are only four parameters for the six equations, the problem is under specified, and, thus, there is no exact solution. The following derivation is only for an approximate solution.]

As $z\to\infty$, the term $[\int_0^z E_n(\xi,t)d\xi]^2\to 1$ and is the only function which does not go to zero. Therefore, we may set

$$A=-r^2/(r+1)^2. \quad (40)$$

For the remaining five equations, we have only three unknowns left. Equation (39) is simplified most radically by setting

$$B\equiv F\equiv 0. \quad (41)$$

This eliminates the effect of the large terms proportional to z^3 and z^4. This choice also removes accidental divergences which would otherwise occur at $r=0.5$ and $r=3.0$ and seem physically unreasonable.

Since there is no solution for C from Eq. (39d) when $r=1$, we use Eq. (39e) to find

$$C=\frac{1}{2}-\frac{1}{2r(r+1)}. \quad (42)$$

Thus, an approximate solution for $\ln c_t$ to second order in α is

$$\ln c_t=\ln c_0'(t)-\frac{x^2}{4D_{t0}t}+\frac{\alpha 2r^{3/2}}{r+1}z\times\int_0^z E_n(\xi,t)d\xi-\frac{\alpha r^{1/2}}{r+1}E_n(z,t)+\frac{\alpha^2E_n^2(z,t)}{2}\left(1-\frac{1}{r(r+1)}\right)-\frac{\alpha^2r^2}{(r+1)^2}\times\left(\int_0^z E_n(\xi,t)d\xi\right)^2. \quad (43)$$

Including the second-order terms in the final iteration of the impurity gives an improved solution for the impurity concentration. Then,

$$c_{imp}=\frac{M}{A(4D_{t0}t)^{1/2}}\mathcal{E}_n(z,t), \quad (44a)$$

where $\mathcal{E}_n(z,t)$ now contains both first- and second-order terms:

$$\mathcal{E}_n(z,t)=\exp\left[-z^2+\frac{\alpha z}{r^{3/2}}\int_0^z E_{n-1}d\xi-\frac{\alpha}{2r^{3/2}}E_{n-1}+\frac{\alpha^2E_{n-1}^2}{4r^3}-\frac{\alpha^2}{4r^3}\left(\int_0^z E_{n-1}d\xi\right)^2\right]\Bigg/\int_{-\infty}^{\infty}\exp\left[-z^2+\frac{\alpha z}{r^{3/2}}\int_0^z E_{n-1}d\xi-\frac{\alpha}{2r^{3/2}}E_{n-1}+\frac{\alpha^2}{4r^3}E_{n-1}^2-\frac{\alpha^2}{4r^3}\left(\int_0^z E_{n-1}d\xi\right)^2\right]dz. \quad (44b)$$

Then, for the tracer, the diffusion coefficient is given by

$$D_t=D_{t0}[1+(\alpha/r^{1/2})\mathcal{E}_n(z,t)] \quad (45)$$

and the logarithm of the tracer concentration, $\ln c_t$, is given by Eq. (43), where the term E_n is everywhere replaced by $\mathcal{E}_n$:

$$\ln c_t=\ln c_0(t)-\frac{x^2}{4D_{t0}t}+\frac{\alpha 2r^{3/2}}{r+1}z\times\int_0^z\mathcal{E}_n(\xi,t)d\xi-\frac{\alpha r^{1/2}}{r+1}\mathcal{E}_n(z,t)+\frac{\alpha^2\mathcal{E}_n^2(z,t)}{2}\left(1-\frac{1}{r(r+1)}\right)-\frac{\alpha^2r^2}{(r+1)^2}\left(\int_0^z\mathcal{E}_n(\xi,t)d\xi\right)^2. \quad (46)$$

The above solution was derived for an infinite strip $-\infty<x<\infty$. The solution for a semi-infinite strip $0\le x<\infty$ is the same except that all normalizations are taken over the interval from $0\le x<\infty$ rather than $-\infty<x<\infty$.

E. Model for Fitting Data from Experiment

For the data analysis of the experiment described in Sec. III the following specific steps were taken.

(i) An approximate solution to the diffusion equation for the impurity concentration,

$$\frac{\partial c_{imp}}{\partial t}=\frac{\partial}{\partial x}\left(D_i\frac{\partial c_{imp}}{\partial x}\right), \quad (47a)$$

where

$$D_i=D_{i0}+\gamma c_{imp}, \quad (47b)$$

was found by iterating three times. The first iteration proceeded from a Gaussian solution:

$$c_{imp}=[M/A(4D_{i0}t)^{1/2}]E_0(z), \quad (48a)$$

where

$$E_0(z)=e^{-z^2}/\int_0^\infty e^{-z^2}dz=2\pi^{-1/2}e^{-z^2} \quad (48b)$$

and

$$z^2=x^2/4D_{i0}t. \quad (48c)$$

(Note that the normalization is over the interval

$0 \le x < \infty$ since the experimental arrangement corresponds to an initial tracer layer on one end of the specimen.)

Then we took

$$D_i = D_{i0}[1 + (\alpha/r^{3/2})E_0(z)] \tag{49a}$$

and found a second solution to Eq. (47a) which was exact to first order in α:

$$c_{imp} = [M/A(4D_{i0}t)^{1/2}]E_1(z, t), \tag{49b}$$

where

$$E_1(z, t) = \exp\left(-z^2 + \frac{\alpha z}{r^{3/2}}\int_0^z E_0(\xi)d\xi - \frac{\alpha}{2r^{3/2}}E_0(z)\right)\Big/ \int_0^\infty \exp\left(-z^2 + \frac{\alpha z}{r^{3/2}}\int_0^z E_0(\xi)d\xi - \frac{\alpha}{2r^{3/2}}E_0(z)\right)dz\,. \tag{49c}$$

An improved approximation for D_i,

$$D_i = D_{i0}[1 + (\alpha/r^{3/2})E_1(z, t)], \tag{50a}$$

gave a third solution to Eq. (47a):

$$c_{imp} = [M/A(4D_{i0}t)^{1/2}]E_2(z, t), \tag{50b}$$

where

$$E_2(z, t) = \exp\left(-z^2 + \frac{\alpha z}{r^{3/2}}\int_0^z E_1(\xi, t)d\xi - \frac{\alpha}{2r^{3/2}}E_1(z, t)\right)\Big/ \int_0^\infty \exp\left(-z^2 + \frac{\alpha z}{r^{3/2}} \times \int_0^z E_1(\xi, t)d\xi - \frac{\alpha}{2r^{3/2}}E_1(z, t)\right)dz\,. \tag{50c}$$

(ii) For $\alpha/r^{3/2} \lesssim 1$ the integral of the first-order solution for c_{imp} (before normalization) has converged to within 1% in three iterations; we next found the solution to Eq. (47a) for the impurity distribution to second order in α, with the impurity diffusivity given by the iterated first-order solution,

$$D_i = D_{i0}[1 + (\alpha/r^{3/2})E_2(z, t)]\,. \tag{51}$$

This gave for the final impurity distribution

$$c_{imp} = [M/A(4D_{i0}t)^{1/2}]\,\mathcal{E}_3(z, t), \tag{52a}$$

where

$$\mathcal{E}_3(z, t) = \exp\left[-z^2 + \frac{\alpha z}{r^{3/2}}\int_0^z E_2 d\epsilon - \frac{\alpha}{2r^{3/2}}E_2 + \frac{\alpha^2}{4r^3}E_2^2 - \frac{\alpha^2}{4r^3}\left(\int_0^z E_2 d\xi\right)^2\right]\Big/ \int_0^\infty \exp\left[-z^2 + \frac{\alpha z}{r^{3/2}}\int_0^z E_2 d\xi - \frac{\alpha}{2r^{3/2}}E_2 + \frac{\alpha^2}{4r^3}E_2^2 - \frac{\alpha^2}{4r^3}\left(\int_0^z E_2 d\xi\right)^2\right]dz\,. \tag{52b}$$

(iii) Using this result as the best estimate for the impurity distribution, the tracer-diffusion coefficient can then be expressed as

$$D_t = D_{t0}[1 + (\alpha/r^{1/2})\,\mathcal{E}_3(z, t)], \tag{53a}$$

and the tracer-penetration profile is given by

$$\ln c_t = \text{const} - \frac{x^2}{4D_{t0}t} + \frac{\alpha 2r^{3/2}}{r+1}z \times \int_0^z \mathcal{E}_3(\xi, t)d\xi - \frac{\alpha r^{1/2}}{r+1}\mathcal{E}_3(z, t) + \frac{\alpha^2}{2}\mathcal{E}_3^2(z, t)\left(1 - \frac{1}{r(r+1)}\right) - \frac{\alpha^2 r^2}{(r+1)^2}\left(\int_0^z \mathcal{E}_3(\xi, t)d\xi\right)^2\,. \tag{53b}$$

This was the model used to find the best fit for the preliminary experiment described in Sec. III.

The above model was used to generate the curves shown in Figs. 1 and 2. The deviation from a Gaussian form is most noticeable at small penetration distances where the integral of the exponential and the exponential terms in Eq. (53b) vary most rapidly. Figure 1 illustrates how the curvature becomes more pronounced as the diffusion time decreases or as the impurity concentration increases, as measured by the parameter $\alpha \propto Mt^{-1/2}$. Since α is inversely proportional to $(D_{t0})^{3/2}$, the effect will increase with decreasing temperature.

The deviation from a Gaussian penetration plot is reduced as r increases as seen in Fig. 2, reflecting the fact that a rapidly diffusing impurity is somewhat homogenized before the tracer can diffuse very far. In this case, although the penetration plot is nearly linear, the limiting slope will not give the true (impurity-free) diffusion coefficient.

For $\alpha \lesssim 0.3$ and $r \gtrsim 0.5$ the solution to first order in α with a Gaussian impurity, Eq. (27a), and the solution to second order in α with a non-Gaussian impurity, Eq. (53b), are indistinguishable. Thus,

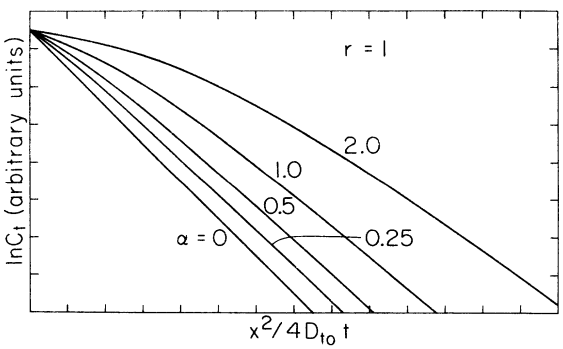

FIG. 1. Penetration plots for a given diffusivity ratio r. The plots become more curved as α increases.

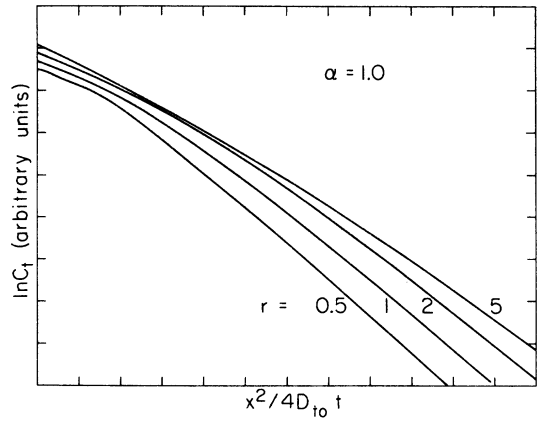

FIG. 2. Penetration plots for a given α. The apparent limiting slope diffusivity increasingly deviates from D_{t0} as r is increased although the apparent curvature near the origin decreases.

the first-order solution with a Gaussian impurity, Eq. (27a), is adequate when α is small.

III. EXPERIMENTAL CHECK

A. Experimental Methods and Results

For a preliminary experiment to test this model three different samples of NaCl with thin evaporated layers of Na^{22} "carrier-free" tracer were simultaneously annealed for different times in a single furnace. Since the samples were diffused simultaneously, any systematic temperature errors would not affect the results, which were concerned with verifying the existence of time-dependent non-Gaussian penetration profiles resulting from the co-diffusion of unknown divalent impurities presumed to be present in the tracer.

The diffusion specimens were prepared from Harshaw high-purity NaCl crystals by cleaving parallelopipeds of dimensions 8×8×3 mm, polishing the cleaved surfaces with a microtome, and then annealing the specimens for 2 h at 750 °C in a dried-argon atmosphere. Na^{22} tracer, purchased in "carrier-free" form as NaCl in H_2O from International Chemical and Nuclear Corporation (ICN), was simultaneously deposited by vacuum evaporation onto one of the 8×8 mm surfaces of each specimen.

The diffusion anneal was done in a linearly wound furnace with a nichrome-block core which could be controlled at a temperature of (616 ± 0.5) °C. The samples were sealed inside quartz capsules filled with an argon atmosphere. The furnace was preheated to 616 °C and allowed to reach equilibrium for several days. The three capsules were placed in symmetric holes in the nichrome-block furnace core. Care was taken to remove a sample quickly in order to minimize cooling and hence warm-up time corrections for the remaining sample(s).

Following the diffusion anneal, the specimens were microtome sectioned and counted in the manner described in the companion paper by Martin, Lazarus, and Mitchell.[2] The over-all accuracy of the measurements, aside from temperature and timing errors (corrections were made for warm-up time), was about ± 5%.

The above model predicts that to first order in the concentration of impurity the deviation from a Gaussian should vary as $t^{-1/2}$. Therefore, the samples were annealed for times that had a ratio of 1 : 4 : 16 so that the parameter $\alpha(t)$ would vary as 1 : 2 : 4. Experimental uncertainties, especially in the ratios of M/A, were estimated as less than 50% in the most extreme case although it is probable that M/A is the same within 10% for the three specimens.

It was expected that when $\ln c_t$ was plotted versus x^2/t for the three cases the longest time would be nearly a straight line (curve a in Fig. 3); the shortest time would be strongly curved (curve c); and the intermediate case would be between the other two. The data shown in Fig. 3 substantiate these expectations.

The model was used to find fits to the data. The values of D_{t0}, α, and r for the best fits are listed

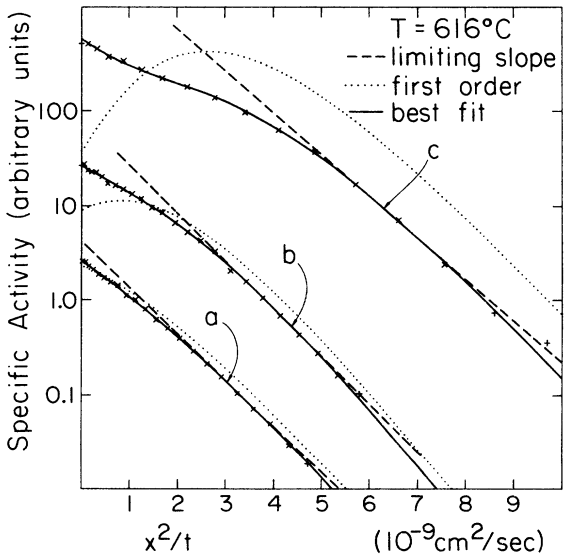

FIG. 3. Penetration profiles of data taken at the same temperature for different times with computer fits (curve a, longest time; curve b, intermediate time; curve c, shortest time). Points labeled + were excluded from the fitting program. The dotted lines show the curves for the given values of α, r, and D_{t0} in which second-order terms α^2 were excluded. $\ln c_0(t)$ for this first-order solution was determined by the normalization condition. The broken line is the limiting slope Gaussian fit.

TABLE I. Na^{22} diffusion in NaCl: best-fit parameters.

Curve in Fig. 3	Time (10^4 sec)	Diffusion coefficient best fit (10^{-10} cm^2/sec)	α	r
a	30.0	1.6	0.67	3.1
b	7.6	1.4	1.36	2.1
c	1.9	1.3	2.52	1.9

in Table I. As seen in Fig. 3 the best fits give random errors. The values for α found for the best fits are 0.67, 1.36, and 2.52 and have a ratio of 1 : 2 : 3.8, which is in remarkable agreement with that predicted from the theory (1 : 2 : 4). Some of the agreement may be fortuitous since it is not known that M/A is identical for the three samples and the "true" self-diffusion coefficient D_{t0}, which should have the same value for all three runs, is found to be 20% higher for the longest-time run than the average D_{t0} for the intermediate and shortest times, although the longest-time run had the least correction, and, therefore, would be expected to be most reliable.

The average diffusivity found for the Na^{22} tracer is 35% lower than the value calculated from Bénière's results for 616 °C.[8] Part of this disagreement may be due to temperature errors since no special precautions were taken to calibrate the absolute temperature in the present measurements. Part may be due to the fact that Bénière did not properly correct for the effects of heterovalent impurities present in his tracer.

The penetration profile for the shortest-time run, curve c in Fig. 3, shows an inflection upward in the near-surface region. The theoretical fit also shows such an inflection, but it is not clear whether this is genuine or if the present model is adequate to explain that extreme case. The inflection could be due to experimental difficulties such as surface hold up.

The identity of the impurity in the present experiment is unknown. Mass spectrographic examination of the Na^{22} tracer disclosed no detectable amount of Mg^{24} or other heterovalent impurity. Other recent work using ICN's "carrier-free" Na^{22} tracer for measurements of the isotope effect in NaCl showed some deviation from a Gaussian in the near-surface region.[1] Analysis of that tracer showed that it contained about 300-μg/ml Ca^{++}, although it is not known whether the Ca^{++} came from the supplier. In one case the non-Gaussian behavior was attributed to the presence of Pb^{++}. Since Na^{22} is made in a cyclotron from a $Mg^{24}(d, \alpha)$ reaction, some residue of Mg could easily be in the tracer. After bombardment the Na^{22} is present only as parts per million in the Mg. Since excited Mg^{24} has a half-life of only 15 sec, it will not show up when the tracer is tested for its radio-chemical purity. The specific activity of pure Na^{22} is 6 Ci/mg. The specific activity of the tracer, however, is only about 10 mCi/mg. From this difference, it seems evident that there must be about 600 neutral atoms per tracer atom. The manufacturer estimated that there are at least 30–150 parts Na^{23} and 100 parts Mg to 1 part Na^{22} in the "carrier-free" Na^{22}.[9]

The diffusivity of Mg in NaCl is unknown. Bénière measured the diffusion of Ca^{++} in NaCl.[8] Interpolating between his points would give $D_{Ca^{++}} = 3.1\times10^{-10}$ cm^2/sec at 616 °C. The average diffusion coefficient for the unknown impurity from the fits of the present data is $3.5(\pm 1.4)\times10^{-10}$ cm^2/sec. Thus calcium, possibly introduced via the desiccant (Drierite) used in storing specimens, magnesium present in the tracer, or both, could be heterovalent impurities.

B. Fitting Procedure

In the present case the diffusivity and initial concentration of the impurity are completely unknown; so the values of r, α, and D_{t0} can only be obtained by finding the best-fit solutions to the measured tracer-penetration profiles. Figures 4–6 show the variances near the absolute minima to illustrate the uncertainty in determining $r = D_{t0}/D_{t0}$ and $F = D_{t0}/D_{ref}$. For the final fit, the computer was programmed to do a much finer search around each absolute minimum. The numbers given in Figs. 4–6 are the variances multiplied by 1000. In determining the variances the first two sections were always ignored. The thickness of the first section was determined by collecting the dust and then weighing it, so probable errors are larger for this point. The second section was also ignored be-

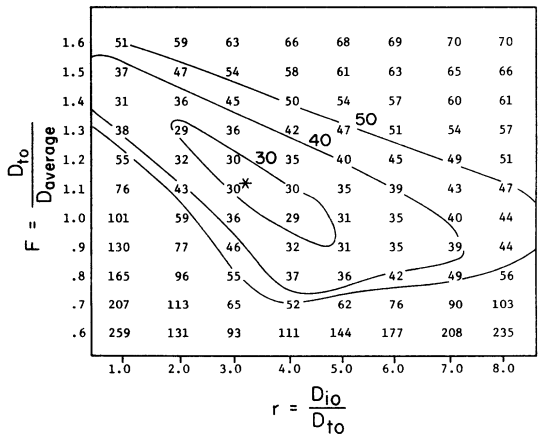

FIG. 4. Field plots of the variances multiplied by 1000 for the longest-time run from the best fits for various r and F.

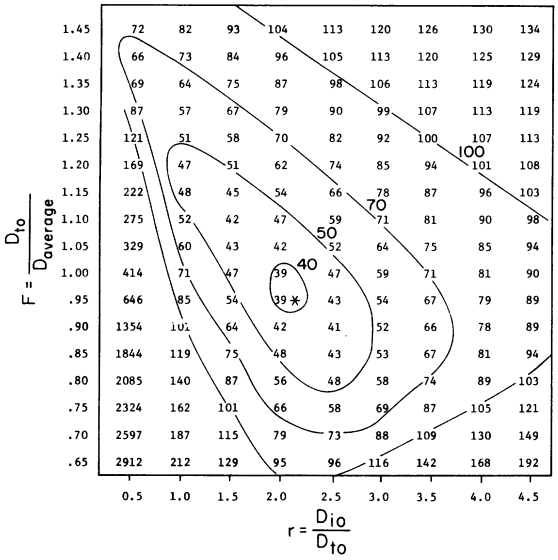

FIG. 5. Field plots of the variances multiplied by 1000 for the intermediate-time run.

cause uncollected dust from the first section might be included in it. The background was generally 80 ± 10 counts per min. Even though at least 10 000 counts were always taken and the background was checked periodically, a variation in the background could introduce significant errors in sections of very low activity, so sections with counting rates less than three times the background were also excluded from the fit. Figure 3 shows these points with a different symbol.

For a given r and F, successive solutions were tried by the computer to give the minimum variance with α as the variable parameter. The value of α was determined to ± 0.001. Since $\ln c_t$ is linear in the normalization constant, $\ln c_0(t)$, values of $\ln c_0(t)$ were easily calculated to minimize the variances. As the lines of equal variance in Figs. 4–6 show, there is a range in r and F which give equivalent fits. Since there were only 15–25 points per profile, there is no statistical guarantee that the "small" fluctuations are random or that the absolute minimum represents the "true fit."

In order to see how α, r, and F were related, plots similar to Figs. 4–6 were generated using simulated data for which α, r, and D_{t0} were known. Simulated data for the Gaussian case ($\alpha = 0$) gave a shallow horizontal valley (i.e., the minimum for any r occurred at the same F) with the variance small and approximately the same in the valley for all r. This is not surprising since α would be small for good fits and the fits would be essentially independent of r. For large $\alpha \sim 3$ the minimum variance followed a constant r as F changed. The variance went up quickly as F moved away from its true value. However, there was still a range of $\pm 5\%$ in D_{t0} for which the variance was less than our experimental errors. For intermediate α's the minimum variances formed a diagonal trough and then eventually followed a constant r. In some cases a range of $\pm 50\%$ in r would produce acceptable variances (less than 0.03 which is our background). This range in r makes precise determination of α or F difficult. Thus, as long as none of the parameters α, r, and F are known *a priori*, it is difficult to determine all three within small limits. Fortunately, the value of F, the correct factor for the tracer diffusivity, can be determined within satisfactorily small limits of uncertainty: e.g., for $\Delta r = \pm 50\%$ and $\Delta\alpha = \pm 30\%$, ΔF does not exceed $\pm 15\%$. The actual data tended to show a smaller range in α, r, and F for acceptable fits.

IV. DISCUSSION

Figures 1 and 2 point out the necessity of great caution in the interpretation of penetration plots that show any downward curvature near the origin. In particular, it is found that one may measure a penetration plot that is nearly linear over several orders of magnitude, but whose slope gives a diffusivity seriously in error. For example, the curve corresponding to $\alpha = 0.5$ in Fig. 1 leads to an error of some 10% in determining the diffusivity from the limiting slope.

Since the ratio of diffusivities in Fig. 1 is unity, the curves can represent the diffusion of divalent tracer ions into monovalent ionic crystals such as Ca^{++} in NaCl. The impurity effect is inherently present in such cases, and so the standard technique of determining the diffusion coefficient from the slope of the penetration profile can be applied

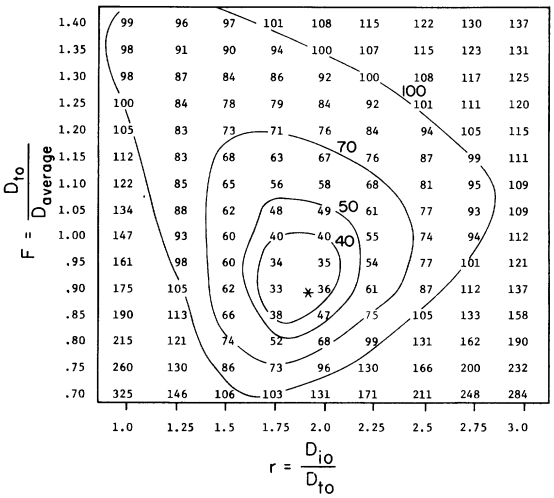

FIG. 6. Field plots of the variances multiplied by 1000 for the shortest-time run.

to interpret diffusion results for divalent ions only in the limit of vanishingly small concentrations or very long anneal times. Curved penetration plots have been seen experimentally for Ca^{++} in NaCl.[5] Numerical calculations based on the Lidiard model have shown that the curvature grows worse as the amount of divalent ion deposited is increased or the diffusion anneal time is decreased which agree with the predictions of our model. Our model was used to fit their simulated curves, showed very precise fits, and, most significantly, showed that the Lidiard model underestimated the needed correction by about a factor of 2.

Particular care should be taken in all tracer-diffusion measurements in insulators to verify that measured diffusion coefficients are actually time independent. Due to experimental difficulties such as surface hold-up which can mask the curvature in the near-surface region, a finding of apparently Gaussian profiles is not always a reliable criterion for assuming that the measured slope is proportional to the actual diffusivity. Often the amount of tracer deposited, and hence the impurity present, is the same for a set of samples in a given laboratory, and the anneal times are chosen to keep the penetration length $(4D_{t0}t)^{1/2}$ about constant. Then α would vary as $(D_{t0})^{-1}$. This effect can lead to measured diffusion coefficients which fit an Arrhenius plot, but which give an activation energy that is too low. Since the divalent ion is likely to have a lower activation energy for diffusion than the monovalent tracer, r is likely to increase as the temperature is decreased. As seen in Fig. 2 the curves for large r show less apparent curvature for a given α, although the limiting slope is in greater error. Thus, the variation with r could tend to reduce the curvature in the near-surface region while increasing the concentration of tracer in the bulk, and thus prevent the effect from showing up as strongly as expected from the increase in α at lower temperatures.

Since the knowledge of the self-diffusion coefficients of the lattice atoms is basic to the understanding of all mass transport phenomena, it is important that the true self-diffusion coefficients are extracted from the curved non-Gaussian profiles rather than assuming that the limiting slope will give the bulk diffusion coefficient. Clearly, this problem applies to tracer diffusion studies in *all* insulating solids, since tracers can never be made absolutely free from impurities. A detailed study of this effect is being undertaken.

---

*Work supported in part by the U.S. Atomic Energy Commission under Contract No. AT(11-1)-1198.

†Present address: Lawrence Livermore Laboratory, Livermore, Calif. 94550.

[1]S. J. Rothman, N. L. Peterson, A. L. Laskar, and L. C. Robinson, J. Phys. Chem. Solids **33**, 1061 (1972).

[2]G. Martin, D. Lazarus, and J. L. Mitchell, following paper Phys. Rev. B **8**, 1726 (1973).

[3]J. E. Hanlon, J. Chem. Phys. **32**, 1492 (1960).

[4]S. J. Rothman, L. W. Barr, A. H. Rowe, and P. G. Selwood, Philos. Mag. **14**, 501 (1966).

[5]F. Bénière, M. Bénière, and M. Chemla, J. Chem. Phys. **56**, 549 (1972).

[6]A. B. Lidiard, Handb. Phys. **20**, 246 (1957).

[7]In Eq. (5), and the following work up to Eq. (26), we have neglected a normalization constant determined by the total amount of tracer deposited. Thus, the derived penetration plots may be shifted up or down by a constant amount.

[8]F. Bénière, thesis (University of Paris-Orsay, 1970) (unpublished).

[9]This estimate was given in a private communication about ICN's "carrier-free" Na^{22} from Richard H. Marsh, Laboratory Director, ICN Chemical and Radioisotope Division.